THE JOURNAL OF BIOLOGICAL CHEMISTRY VOL. 281, NO. 2, pp. 885–895, January 13, 2006

Scanning the Membrane-bound Conformation of Helix 1 in the Colicin E1 Channel Domain by Site-directed Fluorescence Labeling*

Received for publication, October 13, 2005, and in revised form, November 18, 2005 Published, JBC Papers in Press, November 19, 2005, DOI 10.1074/jbc.M511140200

Abdiwahab A. Musse[‡], Jie Wang[§], Gladys P. deLeon[‡], Gerry A. Prentice[‡], Erwin London[§], and A. Rod Merrill[‡1]

From the [‡]Department of Molecular and Cellular Biology, University of Guelph, Guelph, Ontario N1G 2W1, Canada and the [§]Department of Biochemistry and Cell Biology and Department of Chemistry, State University of New York, Stony Brook, New York 11794-5215

Helix 1 of the membrane-associated closed state of the colicin E1 channel domain was studied by site-directed fluorescence labeling where bimane was covalently attached to a single cysteine residue in each mutant protein. A number of fluorescence properties of the tethered bimane fluorophore were measured in the membrane-bound state of the channel domain, including fluorescence emission maximum, fluorescence quantum yield, fluorescence anisotropy, membrane bilayer penetration depth, surface accessibility, and apparent polarity. The data show that helix 1 is an amphipathic α-helix that is situated parallel to the membrane surface. A least squares fit of the various data sets to a harmonic function indicated that the periodicity and angular frequency for helix 1 are typical for an amphipathic α-helix (3.7 ± 0.1 residues per turn and 97 ± 3.0°, respectively) that is partially bathing into the membrane bilayer. Dual fluorescence quencher analysis also revealed that helix 1 is peripherally membrane-associated, with one face of the helix dipping into the lipid bilayer and the other face projecting toward the solvent. Finally, our data suggest that the helical boundaries of helix 1, at least at the C-terminal region, remain unaffected upon binding to the surface of the membrane in support of a toroidal pore model for this colicin.

The colicins are a family of antimicrobial proteins that are secreted by *Escherichia coli* strains under environmental stress, because of nutrient depletion or overcrowding, and these proteins often target sensitive bacterial strains (1). The lethal actions of colicins against their target cells are manifested in a number of different modes that include the following: (i) formation of depolarizing ion channels in the cytoplasmic membrane, (ii) inhibition of protein and peptidoglycan synthesis, and (iii) degradation of cellular nucleic acids (1–7). In this context, the bacterial machinery responsible for colicin biological activity feature important mechanisms that are fundamental to various biological processes. These mechanisms include protein receptor binding, membrane translocation, membrane binding and protein unfolding, membrane insertion, voltage-gated ion channel formation, catalysis, and inhibition of enzymes.

Colicin E1 is a member of the channel-forming subfamily of colicins and is secreted by *E. coli* that harbors the naturally occurring *colE1* plasmid; the whole colicin consists of three functional segments, the translocation, receptor-binding domains, and channel-forming domains. Initially, the receptor-binding domain (8) interacts with the vitamin B_{12} receptor of target cells (9). Following receptor recognition, the translocation domain associates with the *tolA* gene product, which permits the translocation of colicin E1 across the outer membrane and into the periplasm (10). In the periplasm, the channel domain undergoes a conformational change to an insertion-competent state and then inserts spontaneously into the cytoplasmic membrane of the host cell, forming an ion channel. The channel allows the passage of monovalent ions, resulting in the dissipation of the cationic gradients (H^+, K^+, and Na^+) of the target cell, causing depolarization of the cytoplasmic membrane. In an effort to compensate for the membrane depolarization effected by the colicin E1 channel, Na^+/K^+-ATPase activity is increased in the host cell, resulting in the consumption of ATP reserves, without concomitant replenishment (11). The final outcome is host cell death.

A number of techniques have been used to study the topology of the membrane-bound state of colicin E1. Studies of the surface topology of the colicin E1 channel peptide bound to liposomes have been performed using proteases, and it was found that the bound polypeptide is largely sensitized to trypsin proteolysis relative to that in aqueous solution (12). The N-terminal one-third of the 190-residue membrane-bound colicin E1 channel peptide is unbound or loosely bound with the C-terminal two-thirds showing little sensitivity to protease. The membrane-associated closed state of the channel was also studied by depth-dependent fluorescence quenching (13). This approach used Trp as the reporter spectroscopic probe and doxyl-labeled phospholipids as the quencher species. The results from this study were consistent with the presence of only two transmembrane segments in the closed channel and were in agreement with those obtained by Shin *et al.* (14) who conducted an ESR study of spin-labeled cysteine mutants of the channel peptide. Furthermore, the structure and dynamics of the gating mechanism of the colicin E1 channel were studied previously by hydrophobic photolabeling (15) and by site-specific biotinylation (4). Also, the membrane-bound volume of the colicin E1 channel peptide was determined using light scattering analysis and was found to be 177 nm^3, suggesting that the peptide likely has a large hydration shell when membrane-bound (16). Tory and Merrill (17, 18) used a plethora of fluorescence methods to probe the membrane topology of the closed channel state, and they concluded that the monomeric channel features two states that are in rapid equilibrium in which one state is more heavily populated than the other. Furthermore, Zakharov *et al.* (19) proposed that the colicin E1 closed channel exists as a two-dimensional helical array with most of the helices appressed closely to the bilayer surface. Also, Kim *et al.* (20) used ^{15}N-labeled p190 colicin in oriented planar phospholipid bilayers and found that the data were consistent with a single transmembrane helical

* This work was supported by grants from the Natural Sciences and Engineering Research Council of Canada (to A. R. M.) and by National Institutes of Health Grant GM31986 (to E. L.). The costs of publication of this article were defrayed in part by the payment of page charges. This article must therefore be hereby marked "*advertisement*" in accordance with 18 U.S.C. Section 1734 solely to indicate this fact.

[1] To whom correspondence should be addressed: Dept. of Molecular and Cellular Biology, 488 Gordon St., Bldg. 140, University of Guelph, Guelph, Ontario, Canada. Tel.: 519-824-4120 (Ext. 53806); Fax: 519-837-1802; E-mail: rmerrill@uoguelph.ca.

hairpin inserted into the bilayer from each colicin molecule. Moreover, Zakharov *et al.* (21) characterized the kinetic steps involved in the binding and insertion process for the colicin channel domain and later suggested a role for the membrane lipid in the insertion mechanism of colicin E1 (22). Recently, Sobko *et al.* (23) demonstrated that the channel activity of colicin E1 was sensitive to the membrane curvature of the lipid bilayer thus suggesting that the channel may form a toroidal pore in the bilayer. A general mechanism for toxin insertion into membranes was suggested by Elkins *et al.* (11) based on comparison of the x-ray structures of the soluble channel peptides of colicin A and E1.

In this work, we prepared a series of cysteine mutants within helix 1 of the colicin E1 p190 channel domain, and we labeled the Cys residue with the bimane fluorophore. We then used the approach of site-directed fluorescence labeling to scan the membrane-bound topology of the closed state of the channel domain in membrane vesicles. We determined a number of physicochemical and fluorescence properties of the bimane fluorophore tethered at different sites within the channel domain, including fluorescence emission maximum, quantum yield, anisotropy, lifetime, membrane depth, surface accessibility, and apparent polarity. Least squares harmonic wave function analysis of the observed properties of the tethered bimane at various positions along helix 1 reveals that this α-helix is amphipathic and is embedded within the membrane bilayer with its nonpolar face bathing the membrane hydrocarbon core and its polar face interacting with the aqueous solvent.

EXPERIMENTAL PROCEDURES

Expression and Purification of p190His$_6$[2] *Mutants*—The hexahistidine-tagged channel-forming domain of colicin E1 (p190His$_6$ (1)) was purified from a lexA$^-$ strain of *E. coli* (*IT3661*), which contained the pSKHY plasmid that results in constitutive production of the p190 protein. Mutant proteins were purified and characterized as described previously (17). Cells were harvested by centrifugation (5000 × *g*, 5 min) and lysed in 40 ml of loading buffer (50 mM sodium phosphate, 500 mM NaCl, 5 mM imidazole, pH 7.2) at 15,000 p.s.i. using a French press. The lysate was spun down (31,000 × *g*, 30 min), diluted, filtered (2× with two Whatman No. 5 filter paper and 1× with Whatman No. 1 filter paper), and loaded onto Zn^{2+}-charged chelating Sepharose Fast Flow resin (GE Healthcare, Baie D'Urfé, Quebec, Canada). The loaded column was washed with 20 bed volumes of the loading buffer and subsequently with a wash buffer (50 mM sodium phosphate, 500 mM NaCl, 15 mM imidazole, pH 7.2). The protein was eluted using an elution buffer (50 mM sodium phosphate, 150 mM NaCl, 25 mM EDTA, pH 7.2) and dialyzed against 50 mM sodium phosphate, 150 mM NaCl, pH 7.0 buffer. The purity of the protein samples was assessed by SDS-PAGE, and all mutant proteins were at least 90% pure. The protein concentration was determined by UV absorption at 280 nm using an extinction coefficient of 28,590 M^{-1} cm^{-1} (an $\epsilon_{M,\,280}$ of 27, 310 M^{-1} cm^{-1} was used for Y356C and Y363C).

Fluorescence Labeling of p190H Mutants—The fluorescent labeling of all mutants was accomplished using a 20-fold molar excess of monobromobimane (mBBr; Molecular Probes, Eugene, OR) in 200 mM Tris-HCl, pH 8.1, at room temperature for 2 h. Prior to the addition of the fluorescent label, protein samples were reduced with a 5-fold molar excess of dithiothreitol for 30 min. The labeled protein was separated from free label using a pre-packed Econo-Pac 10DG column (Bio-Rad) equilibrated and eluted with phosphate-buffered saline buffer, pH 7.0. The absorbance spectrum of each labeled protein was obtained using a Cary 300 UV-visible dual-beam spectrophotometer (Varian Instruments, Mississauga, Ontario, Canada). The stoichiometry of the protein-bimane conjugation reaction was calculated as the molar ratio of conjugated bimane and labeled proteins. The molar concentrations of the conjugated bimane and protein were determined from the absorbance at 380 and 280 nm using the molar extinction coefficients (ϵ_M) of 5,000 and 28,590 M^{-1} cm^{-1}, respectively (an $\epsilon_{M,\,280}$ of 27,310 M^{-1} cm^{-1} was used for Y356C and Y363C). The contribution to the absorbance at 280 nm from bimane was accounted for before the calculation of the protein concentrations. The labeling efficiency of all proteins was nearly 100%.

In addition to the introduced cysteine residues, all p190His$_6$ possessed one additional cysteine residue, Cys-505, which is buried within the core of the protein. Labeling of the buried sulfhydryl side chain of Cys-505 has been shown previously to require the partial unfolding of the protein (24). Incubation of excess mBBr with wild-type (WT) p190His$_6$ resulted in negligible background labeling (<1%). Therefore, given the near 1:1 stoichiometry of the labeling reactions and the lack of bimane labeling of the WT protein, all the fluorophores were presumed to be attached to the introduced cysteine residues, and the buried Cys-505 did not participate in the labeling reaction.

Preparation of Vesicles—Large unilamellar vesicles (LUVs) were prepared from 1,2-dioleoyl-*sn*-glycero-3-phosphocholine and 1,2-dioleoyl-*sn*-glycero-3-[phospho-rac-(1-glycerol)] (Avanti Polar Lipids, Alabaster, AL) in 60:40% molar ratio by extrusion through a 100-nm polycarbonate filter (Lipofast, Aventin Inc., Ottawa, Ontario, Canada) in 20 mM dimethylglutaric acid, 130 mM NaCl, pH 4.0, and phospholipid concentration was determined using the Bartlett assay for phosphorus as described earlier (17).

Steady-state Fluorescence Measurements of Mutants—All steady-state fluorescence measurements, except for the dual quencher experiments, were made with a PTI-Alphascan-2 spectrofluorometer (Photon Technologies Inc., South Brunswick, NJ) equipped with a thermostated cell holder. Unless otherwise stated, a 2.5–4.0 μM protein sample in 20 mM dimethylglutaric acid, 130 mM NaCl, pH 4.0, in the presence or absence of excess LUVs (800 μM, final concentration), was used for all measurements. The temperature was maintained constant at 22 °C.

Structural and Functional Assessments—The folding properties of all mutants were examined by monitoring the intrinsic tryptophan fluorescence of each protein compared with the WT. Trp fluorescence emission spectra of labeled and unlabeled mutant proteins in pH 7.0 phosphate-buffered saline buffer were obtained using 295-nm excitation light. The excitation and emission slit widths were 2 and 4 nm, respectively, and the fluorescence emission was scanned from 305 to 450 nm. Corrections were made for the appropriate blanks and for the wavelength-dependent bias of the optical and detection systems. The fluorescence emission maximum ($\lambda_{em,\,max}$) values were determined from the first derivative of the smoothed spectra. These data were used to assess the structural integrity of the mutant proteins as compared with the WT protein. In addition, the *in vitro* channel activity of all mutants was also assayed as described earlier (24).

Bimane Fluorescence Emission Spectra—The steady-state fluorescence emission spectra, in the presence or absence of LUVs, were measured from 395 to 600 nm while exciting at 381 nm. The excitation and emission slit widths were kept at 2.0 and 4.0 nm, respectively. To minimize vesicle light scattering, a 390 nm cut-off filter (Oriel Corporation, Rockford, IL) was placed in the emission light path. The signal from

[2] The abbreviations used are: p190His$_6$, colicin E1 190-residue channel domain with an N-terminal His$_6$ tag; mBBr, monobromobimane; WT, wild type; LUVs, large unilamellar vesicles; Q_F, fluorescence quantum yield; bimane-Cys, bimane-labeled *N*-acetylcysteine; *Q* ratio, the ratio of quenching by KI to that by 10-DN; SASA, solvent-accessible surface area; 10-DN, 10-doxylnonadecane.

solvent blank (buffer or LUVs in buffer) was subtracted from the sample fluorescence, and the spectra were corrected for the wavelength dependence of the instrument response.

Quantum Yield Measurements—The bimane fluorescence quantum yields (Q_F), in the presence and absence of LUVs, of all mutants were obtained using quinine sulfate ($Q_F = 0.53$ in 0.1 N H_2SO_4) as a quantum standard (25). The excitation wavelength was set at 360 nm while scanning the emission spectra from 370 to 600 nm in 1 nm increments. The excitation and emission slit widths were 4.0 and 6.0 nm, respectively. The absorbance at the excitation wavelength for the various samples ranged between 0.05 and 0.1. To minimize light scattering effects, the excitation light was vertically polarized, and the emission was detected at 54.7° (magic angle). The signal from the solvent blank (buffer or LUVs in buffer) was subtracted from the sample fluorescence, and the spectra were corrected for the wavelength dependence of the instrument response. Using the wavelength-integrated fluorescence intensities and the optical densities at the excitation wavelength of the sample and the reference, the quantum yield was calculated as shown in Equation 1,

$$Q_F = Q_R \frac{I}{I_R} \frac{A_R}{A} \qquad \text{(Eq. 1)}$$

where Q_R is the quantum yield of the reference sample; I and I_R are the integrated fluorescence intensities of the sample and the reference, respectively; A and A_R are the optical densities, at the excitation wavelength, of the sample and the reference, respectively. The reported values represent the mean of at least three determinations.

Steady-state Fluorescence Anisotropy Measurements—The steady-state fluorescence anisotropy (r) measurements were made using "T-format" detection by simultaneously comparing the intensities of the vertically (I_{VV}) and horizontally (I_{VH}) polarized emitted light when the sample was excited with a vertically polarized light. By using the I_{VV} and I_{VH} fluorescence intensities, the anisotropy (r) was calculated as shown in Equation 2.

$$r = \frac{I_{VV} - GI_{VH}}{I_{VV} + 2GI_{VH}} \qquad \text{(Eq. 2)}$$

The "G" instrumental factor, measured as I_{HV}/I_{HH}, was determined from the intensities of the vertically (I_{HV}) and horizontally (I_{HH}) polarized emitted light from horizontally polarized excitation light. For all measurements, the excitation was set at 381 nm (4 nm slit width), and emission was collected at 470 nm (10 nm slit width) with a signal integration time of 30 s. Each anisotropy value is the mean of three determinations. A solvent blank (buffer or LUVs in buffer) was subtracted from each intensity reading prior to the calculation of the anisotropy value.

Depth-dependent Dual Fluorescence Quenching Measurements Using Iodide and 10-Doxylnonadecane—For the depth measurement of bimane-labeled residues within the bilayer, iodide and 10-doxylnonadecane (10-DN) quenching of bimane was measured as described previously (26, 27). To measure iodide quenching (F_{KI}), the fluorescence of samples was measured on a Spex Tau-2 Fluorolog Spectrofluorimeter (Jobin Yvon Inc., Edison, NJ) in ratio mode using semi-micro quartz cuvettes (excitation path length 10 mm, emission path length 4 mm) containing 100 μM LUVs and 7.5 μg of protein or LUVs only (background). F_{KI} was determined after the addition of a 50-μl aliquot of an aqueous solution from a 1.7 M KI and 0.85 mM $Na_2S_2O_3$ stock solution. The initial fluorescence of the samples in the absence of the quencher (F_o) was obtained from equivalent samples in which a 50-μl aliquot of 0.85 mM $Na_2S_2O_3$ was added to each sample instead of KI. The excitation wavelength was set at 375 nm while observing the emission intensity at 467 nm. The excitation and emission slit widths were 2.5 and 5.0 nm, respectively. To measure the efficiency of 10-DN quenching, membrane-bound protein or vesicles lacking protein were prepared as described above except that the 10-DN quencher-containing LUVs contained 10 mol % of 10-DN. The samples were allowed to equilibrate for 30 min at 24 °C before measurement.

Calculation of the Iodide to 10-DN Q Ratio—The ratio of quenching by KI to that by 10-DN (Q ratio) was used to determine bimane depth in lipid bilayers. The Q ratio was calculated from Equation 3,

$$Q - \text{ratio} = \frac{((F_o/F_{KI}) - 1)}{((F_o/F_{10-DN}) - 1)} \qquad \text{(Eq. 3)}$$

where F_o is the fluorescence of a sample lacking quencher, and F_{KI} and $F_{10\text{-}DN}$ are the fluorescence intensities in the presence of KI or 10-DN, respectively.

Sensitivity of the Fluorescence Parameters of Bimane to Solvent Polarity—The sensitivity of the bimane fluorescence to solvent polarity was assessed using *N*-acetylcysteine conjugated with bimane (bimane-Cys) as a probe. Bimane-Cys was produced by reacting mBBr with 10-fold molar excess of *N*-acetylcysteine in 100 mM NH_4HCO_3, pH 8.1, for 1 h. The reaction mixture was lyophilized overnight and subsequently resuspended in dioxane:water mixtures of 0 to 100% (v/v) dioxane. The fluorescence emission and lifetime of bimane-Cys (2 μM bimane-Cys) samples in dioxane:water mixtures of different dielectric constants ($\epsilon = 2.3–80$) were determined.

Analysis of the Solvent-accessible Surface Area (SASA)—The solvent accessibility of each residue in helix 1 of $p190H_6$ (347–365) to a 1.4-Å probe (water) was calculated using the Web-based program GETAREA 1.1 (www.scsb.utmb. edu/getarea/area_ man.html) (28) and the crystal structure coordinates of the WT p190 colicin E1 (11).

Predicting Secondary Structure from Fluorescence Parameters—The secondary structure elements within the colicin E1 channel domain were predicted from the observed fluorescence parameters using a method adopted from Cornette *et al.* (29). In brief, the periodicity and the angular frequency of the observed fluorescence parameters were obtained through a least squares fit of the data using the harmonic wave function as shown in Equation 4,

$$y = a \cdot \sin\left(2\pi\left(\frac{x+b}{p}\right)\right) + c \qquad \text{(Eq. 4)}$$

where a is the amplitude; b is the phase; p is the period; and c is an offset value. All calculations were made using an Excel 2002 template spreadsheet developed in-house by Dr. Uwe Oehler.

RESULTS

The primary sequence of the colicin E1 channel domain, $p190H_6$, is shown in Fig. 1*A*, and the protein sequence, including helix 1 in the water-soluble structure that was Cys-scanned, is indicated by the *downward facing brace*. Additionally, the overall topology of helix 1 within $p190H_6$ and also the locations of the inserted Cys residues are shown as *spheres* that correspond to the C-α carbon of each residue (Fig. 1*B*). The channel domain is a bundle of 10 α-helices that is composed of four antiparallel helical pairs that include helix 1 matched with helix 2 (layer A, see Fig. 1*B*), a helical segment that forms a strap across the structure (helices 5_a and 5_b), and the C-terminal helix (helix 10). Although it is believed that the helices within layer A of the channel domain are not

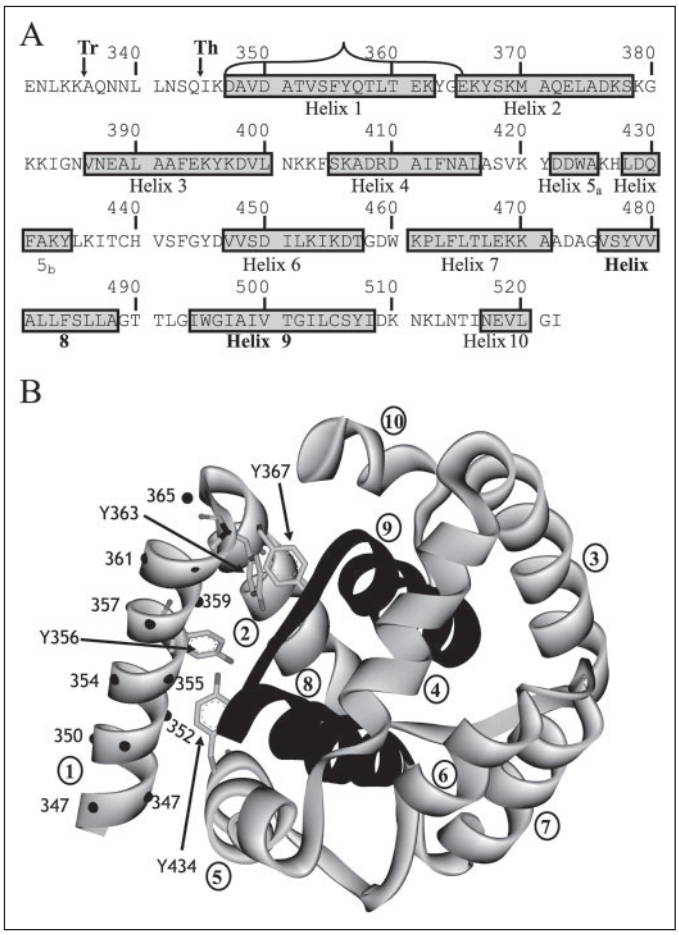

FIGURE 1. **Schematic representation of the channel domain of colicin E1.** *A,* the primary sequence and the secondary structure of the channel-forming domain of colicin E (p190). The hexahistidine-tagged was incorporated immediately before Glu-331 to form the p190His$_6$ channel peptide. *Highlighted in braces* are the residues corresponding to the Cys substitutions. The tryptic and thermolytic digestion sites of the channel-forming domain are shown as *Tr* and *Th*, respectively. *B,* the ribbon topology diagram of the 2.5 Å crystal structure of the p190 peptide (11). The overall architecture of the structure consists of 10 helices, a hydrophobic helical hairpin (helices 8 and 9, *black*) surrounded by eight amphipathic helices that is arranged in a three-layered sandwich helical bundle: layer A, *helices 1, 2,* and *10*; layer B, *helices 8, 9,* and *5*; layer C, *helices 3, 4, 6,* and *7* (11). The locations of the cysteine mutation sites are highlighted with *numbers* and/or *black spheres* that represent the α-carbon of each substituted residue. The *dark colored* α-*helices* are *helices 8* and *9*, which serve as a membrane-anchoring helical hairpin in the membrane-associated closed channel state of the protein. *Highlighted* in side chain *stick format* are Tyr-356, Tyr-363, Tyr-367, and Tyr-434.

involved in direct contact with the membrane, they may play an important role in channel formation (11). The angle between helices 1 and 2 is about 33° and results in helix 1 extending away from the body of the molecule. This region is believed to serve as the hinge to provide sufficient flexibility to allow rotation to the appropriate docking orientation on the cytoplasmic membrane of the bacterial host (11).

Characterization of WT and Mutant p190H$_6$—The N-terminal hexahistidine tag has been incorporated previously in the channel domain of colicin A and N, for ease of purification (30). Structural and functional characterizations of His-tagged colicin A and N channel domains have shown that the incorporation of the hexahistidine tag did not significantly alter the channel properties of these two proteins (30). In the present study, we used intrinsic Trp fluorescence as a probe of protein conformation as well as *in vitro* channel activity analysis to assess the impact of how the engineered hexahistidine tag, the introduction of cysteine residues, and the bimane labeling affected the structural and functional integrity of the protein. Previously, membrane binding analysis of the p190H$_6$ revealed that the dissociation constant (K_d) for membrane association of the His-tagged channel peptide did not vary significantly from the untagged, thermolytic channel domain of WT colicin E1. Also, the binding of WT p190H$_6$ to anionic LUVs under conditions (pH 4, ionic strength, $I \sim 0.1$ M, anionic lipid content = 40%) for which the protein has the highest activity was assayed as described earlier (24, 31). The observed binding parameters, $n = 32-45$ (lipid molecules bound per protein) and $K_d = 0.8-1.2$ nM, are in good agreement with earlier results for the WT colicin thermolytic channel peptide (24, 31). Moreover, the Trp $\lambda_{em,\,max}$ of all mutant proteins (bimane-labeled and unlabeled proteins) showed values that were similar with those of the WT p190H$_6$ (Table 1), indicating that the global folding pattern of the mutants was similar or did not differ significantly from that of the WT thermolytic channel domain. The *in vitro* channel activities of all p190H$_6$ WT and mutant proteins were also comparable with the previously characterized thermolytic WT channel domain (data not shown) (24).

TABLE 1
Summary of the Trp λ_{em} max values observed for the WT and the bimane-labeled/unlabeled Cys mutants of colicin E1 channel peptide

Sample	$\lambda_{em,\,max}$[a]	
	Unlabeled	Labeled
	nm	
WT	318 ± 1	
D347C	319 ± 1	319 ± 1
A348C	318 ± 1	318 ± 1
V349C	319 ± 1	318 ± 0.5
D350C	323 ± 1	318 ± 1
A351C	319 ± 1	319 ± 1
T352C	319 ± 1	318 ± 1
V353C	319 ± 1	318 ± 1
S354C	319 ± 1	318 ± 1
F355C	322 ± 1	318 ± 1
Y356C	322 ± 2	319 ± 1
Q357C	320 ± 1	317 ± 1
T358C	319 ± 1	319 ± 1
L359C	327 ± 0.5	323 ± 1
T360C	321 ± 1	321 ± 1
E361C	320 ± 0	319 ± 1
K362C	323 ± 0.5	321 ± 0.5
Y363C	319 ± 1	318 ± 1
E365C	322 ± 1	319 ± 1

[a] Values shown are the means ± the S.D. from at least triplicate measurements.

The Bimane Fluorescence Emission Maxima of p190H$_6$ Cys Mutants—Fig. 2*A* shows the bimane $\lambda_{em,\,max}$ of the p190H$_6$ Cys mutants in the water-soluble state. On the basis of the bimane $\lambda_{em,\,max}$ values, the probe attachment sites of the soluble p190H$_6$ can be divided into three groups. Group I consisted of mutant proteins with red-shifted $\lambda_{em,\,max}$ (≥470 nm), D347C, A348C, V349C, D350C, V353C, S354C, Q357C, T358C, T360C, E361C, K362C, and E365C. For group II, A351C, Y356C, and Y363C showed slightly intermediate $\lambda_{em,\,max}$ values (469 nm). For group III, the $\lambda_{em,\,max}$ of mutants T352C, F355C, and L359C were distinctly blue-shifted, ranging from 460 to 465 nm, as compared with group I. Such differences in the $\lambda_{em,\,max}$ values of the attached bimane fluorophore and the overall sinusoidal profile are consistent with the amphipathic α-helical nature of this segment in the soluble state of the protein.

Fig. 2*B* illustrates the side chain SASA that corresponds to each inserted Cys residue within the p190H$_6$ channel peptide. SASA was calculated in order to correlate quantitatively the measured $\lambda_{em,\,max}$ with the solvent accessibility of each thiol site. The pattern of the $\lambda_{em,\,max}$ (Fig. 2*A*) and SASA (Fig. 2*B*) appear to correlate very well. Residues with high solvent accessible areas (≥50Å^2) showed consistently higher $\lambda_{em,\,max}$ values (≥470 nm), whereas sites with low solvent accessibility (≤10 Å^2) displayed blue-shifted $\lambda_{em,\,max}$ values (<470 nm).

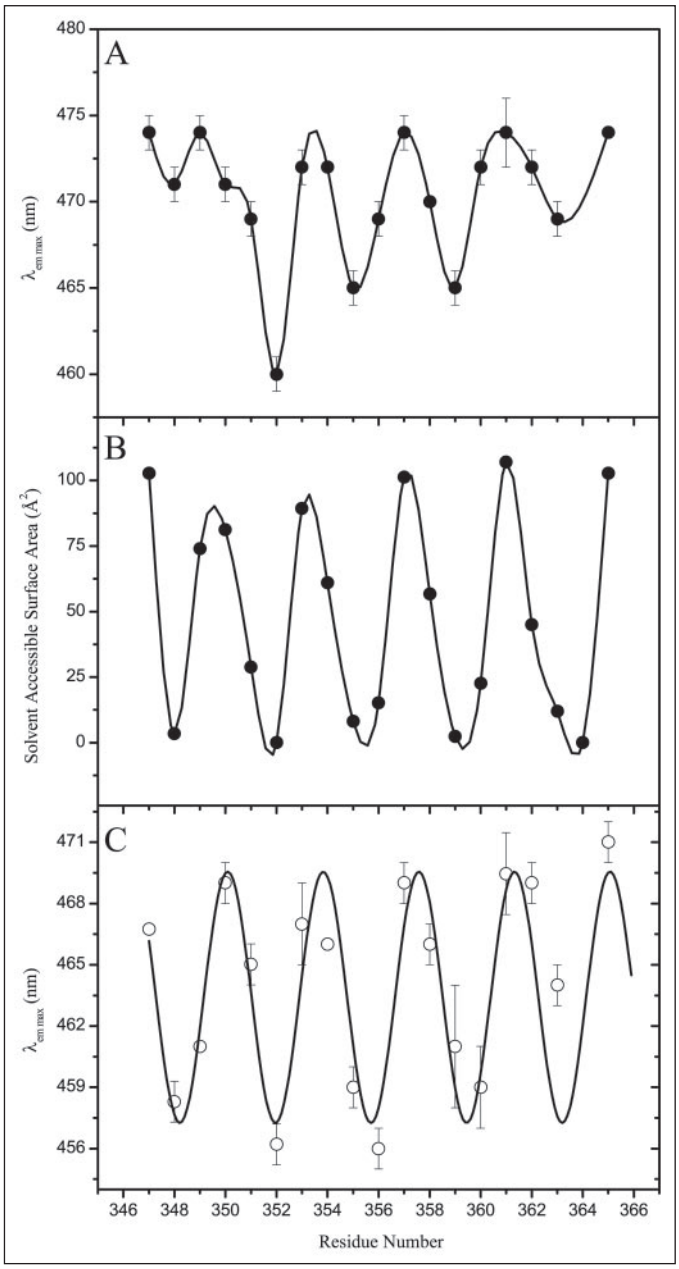

FIGURE 2. **The fluorescence emission maximum ($\lambda_{em,\,max}$) of bimane-labeled Cys mutants of colicin E1 channel domain and the corresponding solvent accessibility of helix 1 within the soluble channel peptide.** *A,* the bimane $\lambda_{em,\,max}$ values (●) of the Cys mutants of the soluble channel domain. *B,* side chain SASA of the Cys-substituted residues within helix 1 of the soluble channel domain. Solvent-accessible surface areas were calculated from the coordinates of the crystal structure of soluble p190 peptide using 1.4-Å probe as described under "Experimental Procedures." *C,* the bimane $\lambda_{em,\,max}$ values (○) of the membrane-associated Cys mutants fitted, through nonlinear least square, to a harmonic wave function ($r^2 = 0.99$).

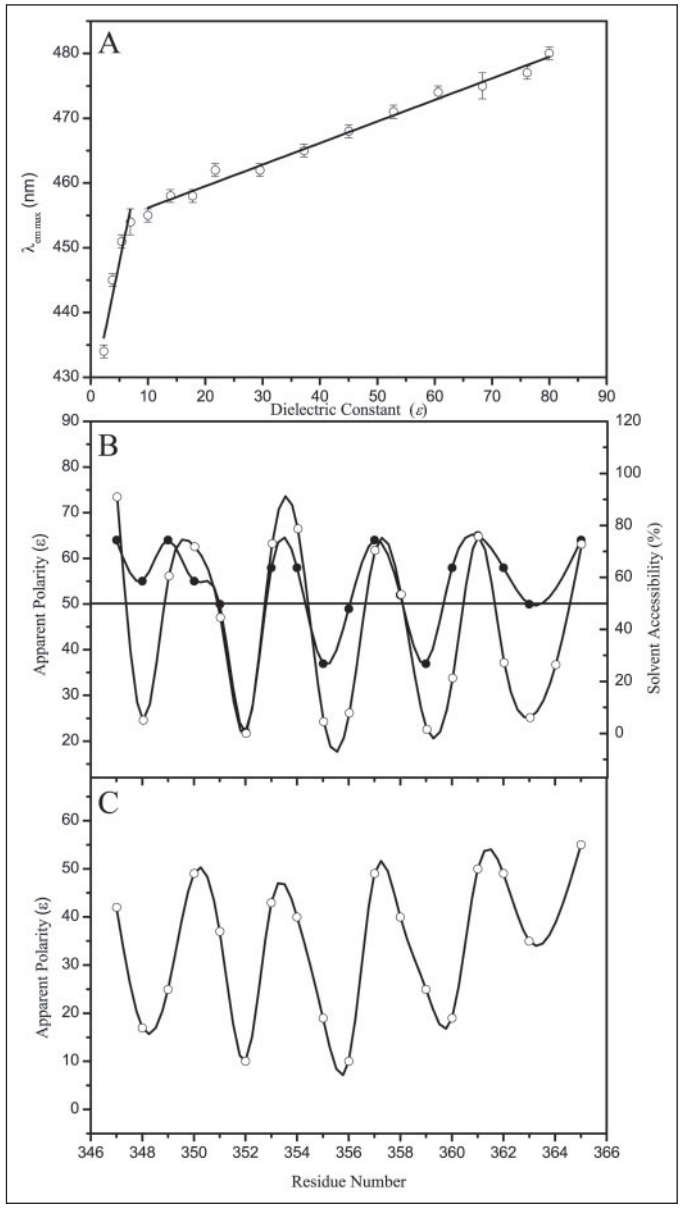

FIGURE 3. **Solvent sensitivity of the $\lambda_{em,\,max}$ of a model compound, bimane-Cys, and the calculated solvent polarities of the bimane-labeled Cys mutants.** *A,* the linear dependence of the $\lambda_{em,\,max}$ of bimane-Cys on the dielectric constant (ϵ) of the solvent. *B,* comparison of the calculated soluble state side chain solvent accessibility (○) and the apparent local environment polarity (●) of the bimane-labeled Cys within helix 1. The solvent accessibility of each residue was calculated as the ratio of the side chain surface area as estimated from the crystal structure (Fig. 2*B*) and the expected theoretical value of each residue in the random coil tripeptide, Gly-*X*-Gly. Residues with solvent accessibility ratios above 50% (—) are considered to be surface-exposed, whereas residues with ratios ≤20% are buried. *C,* the apparent local environment polarity values (○) of the bimane-labeled Cys at each substituted site in the membrane-associated state of all mutants.

The nonlinear least squares fits to a harmonic wave function of the $\lambda_{em,\,max}$ values for helix 1 residues (347–365) in the membrane-associated state of p190H_6 are shown in Fig. 2*C*. The pattern of the profile for the membrane-bound state of helix 1 is very similar to that of the solution conformation (Fig. 2*A*), indicating that the amphipathic α-helical nature of this segment of the protein is not significantly affected upon binding to the membrane. The observed $\lambda_{em,\,max}$ values of the attached bimane probes within helix 1 in the membrane-bound state are blue-shifted when compared with their corresponding values in the solution state, reflecting the change in the polarity of the local environment of helix 1 upon membrane association.

Sensitivity of the Steady-state Fluorescence to the Local Environment—In order to correlate the bimane $\lambda_{em,\,max}$ for all the mutant proteins with the apparent polarity of the local environment of the attachment sites, a standard "apparent" polarity scale curve (Fig. 3*A*) was generated by determining the $\lambda_{em,\,max}$ of a bimane-*N*-acetyl-Cys in a dioxane:water mixed solvent system with variable dielectric constants. Similar apparent polarity standard curves have been reported previously for bimane-labeled proteins and arguably provide quantification of instrument-independent apparent polarity scales (32). Consistent with the earlier observations of Mansoor *et al.* (32), the $\lambda_{em,\,max}$ values of

Cys-bimane varied linearly with the dielectric constant of the bulk solvent. Two linear regions are observed in the following two dielectric constant categories: (*a*) $\epsilon = 2–7$, and (*b*) $\epsilon = 10–80$ (Fig. 3*A*). Linear least squares analysis of the correlations between the $\lambda_{em,\,max}$ values and the dielectric constant (D) of the bulk solvent of these two regions are summarized as follows: (*a*) for $\epsilon = 2–7$, $\lambda_{em,\,max} = 4.28\ (nm/\epsilon) \times D + 426.3\ (nm)$, and (*b*) for $\epsilon = 10–80$, $\lambda_{em,\,max} = 0.33\ (nm/\epsilon) \times D + 452.8\ (nm)$. The slope and the y intercept values of the above relations are comparable with the values reported by Farrens and co-workers (32).

For the purpose of quantitatively discriminating buried amino acid side chains from the surface-exposed residues, we compared the calculated apparent polarity profile (Fig. 3*B*, ●) of helix 1 (347–365) in the soluble state of $p190H_6$ and the corresponding solvent accessibility of each side chain (Fig. 3*B*, ○). Solvent accessibility is determined as a percent ratio of the accessible surface area of each residue, calculated from the coordinates of the crystal structure, and the expected, exposed surface area of that side chain in a random coil conformation (28). Residues with ≤20% relative solvent accessible areas are assigned as buried, whereas residues with ≥50% solvent accessibility (*solid horizontal line*) are considered as surface-exposed (28). The calculated local environment apparent polarity of the scanned sites and the corresponding solvent accessibility value of helix 1 residues generally show excellent agreement, as expected. An exception here is the apparent discontinuity between the calculated apparent local environment polarity and estimated solvent accessibility of Cys-substituted residues located at the N- and C-terminal regions of helix 1 (Ala-348, Thr-360, Lys-362, and Tyr-363). This discrepancy may at least partially be reconciled based on the following arguments. It was shown previously that the N terminus of helix 1 was largely disordered in the crystal structure and that Ala-348 formed the boundary between the disordered and ordered segments of the helix (11). The elevated apparent polarity of A348C could be the consequence of increased disorder within the helix 1 region induced by the Cys substitution and the subsequent bimane labeling at that site. Furthermore, the residues located at the C terminus of helix 1, Thr-360, Lys-362, and Tyr-363 are located near a tightly packed tertiary structure consisting of a two-residue turn between helices 1 and 2 that involve substantial tertiary contacts. It is likely that the increased solvent exposure of the probes at these sites may be because of a local structural perturbation as a consequence of the introduced mutation and labeling. Finally, the small fluorescence anisotropy of bimane attached at these Cys sites (Fig. 4, *A* and *B*) is consistent with this explanation (see "Fluorescence Anisotropy" under "Results").

Surface Orientation and Membrane Disposition of Helix 1—Fig. 3*C* illustrates the apparent local environment polarity (○) of the labeled membrane-bound mutant proteins. The apparent polarities of the bimane-labeled mutant proteins A348C, V349C, T352C, F355C, Y356C, L359C, and T360C ($\epsilon = 10–25$) are relatively consistent with residues positioned at the interfacial layer of the membrane. This is in contrast to the calculated apparent polarity of bimane linked to the mutant proteins D347C, D350C, A351C, V353C, S354C, Q357C, T358C, E361C, K362C, Y363C, and E365C, which showed ϵ values (35–55) well outside that of the interfacial layer of the membrane. As such, these two groups of mutants constitute the residues involved in the bilateral disposition along the surface of the membrane of helix 1 within the membrane-bound channel domain. Furthermore, the measured apparent polarities of the most buried (nonpolar) bimane attachment sites are well beyond the accepted ϵ values ($\epsilon = 2–4$) for the interior of the membrane, thus excluding the possibility of a transmembrane topology for this segment of the protein in the closed channel state.

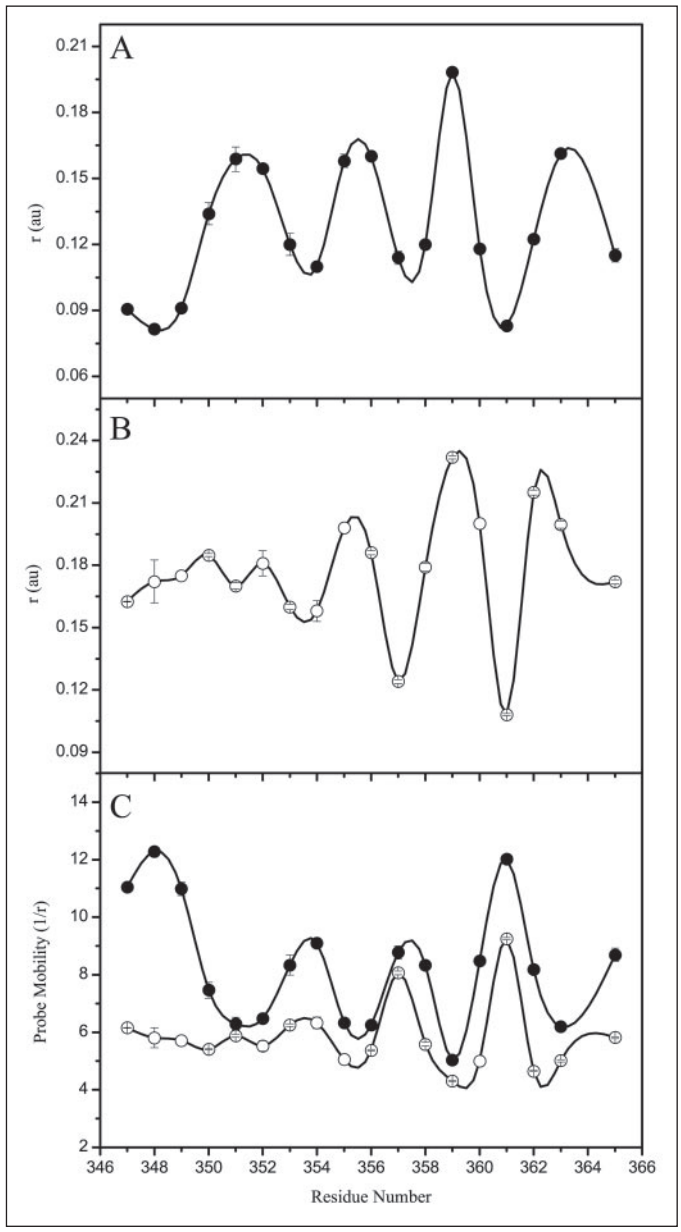

FIGURE 4. **The steady-state fluorescence anisotropy and probe mobility of bimane-labeled Cys mutants of the colicin E1 channel domain.** *A*, the fluorescence anisotropy (●) of the bimane-labeled Cys mutants in the soluble state. *B*, the membrane-associated state fluorescence anisotropy (○) of the bimane-labeled Cys mutants. *C*, comparison of the probe mobility of the bimane-labeled Cys mutants in the membrane-associated (○) and soluble-state (●) conformations. Probe mobility of each site was calculated as the inverse of the fluorescence anisotropy.

Fluorescence Anisotropy—Fig. 4*A* shows the bimane fluorescence anisotropy observed for mutant proteins in the water-soluble state. The observed anisotropy of bimane at the attachment sites followed a similar pattern to the $\lambda_{em,\,max}$ and apparent polarity data. Mutant proteins corresponding to surface-exposed helix 1 sites, D347C, A348C, V349C, D350C, V353C, S354C, Q357C, T358C, E361C, and E365C, showed relatively low fluorescence anisotropy values ($r = 0.081–0.134$). This is in contrast to the observed anisotropy ($r = 0.154–0.198$) for mutants characterized to be solvent-inaccessible, T352C, F355C, Y356, and L359C, based on their apparent polarities and the corresponding solvent accessibilities (Fig. 3*B*). Furthermore, bimane tethered to mutants proteins A348C and E360C showed anisotropy values consistent with those of surface-exposed substituted sites. This is also in agreement

TABLE 2

Summary of the fluorescence quantum yields (Q_F) of bimane-labeled Cys mutants of the colicin E1 channel peptide in the soluble and membrane-associated states

Sample	Q_F[a]	
	Soluble	Membrane-associated
Cys-bimane	0.18 ± 0.00	
D347C	0.22 ± 0.00	0.35 ± 0.00
A348C	0.24 ± 0.01	0.31 ± 0.01
V349C	0.20 ± 0.00	0.52 ± 0.01
D350C	0.12 ± 0.00	0.19 ± 0.00
A351C	0.05 ± 0.00	0.12 ± 0.00
T352C	0.21 ± 0.01	0.13 ± 0.00
V353C	0.05 ± 0.00	0.12 ± 0.00
S354C	0.23 ± 0.01	0.31 ± 0.01
F355C	0.10 ± 0.00	0.32 ± 0.00
Y356C	0.11 ± 0.00	0.40 ± 0.01
Q357C	0.11 ± 0.00	0.13 ± 0.00
T358C	0.21 ± 0.00	0.28 ± 0.01
L359C	0.09 ± 0.00	0.28 ± 0.00
T360C	0.19 ± 0.00	0.22 ± 0.00
E361C	0.23 ± 0.00	0.20 ± 0.00
K362C	0.18 ± 0.00	0.21 ± 0.00
Y363C	0.21 ± 0.00	0.57 ± 0.02
E365C	0.18 ± 0.00	0.27 ± 0.01

[a] Q_F values were determined using quinine sulfate (Q_F = 0.53 in 0.1 N H_2SO_4) as the quantum standard. Values shown are the means ± S.D. of at least triplicate measurements.

with the red-shifted $\lambda_{em,\,max}$ values for those two sites (Fig. 2*C*). The fluorescence anisotropy of Y363C and A351C mutants (r = 0.161 and 0.159, respectively), both of which exhibit red-shifted $\lambda_{em,\,max}$ values and show apparent local solvent polarities characteristic of surface-exposed sites, suggests a high degree of probe immobilization more consistent with those of buried residues within the protein. However, a simple, possible explanation for these elevated fluorescence anisotropy values may be that the bimane tethered at these sites may be restricted because of tertiary structure contacts.

Fig. 4*B* shows the bimane fluorescence anisotropy of the mutant proteins upon membrane association. The residue pattern for the membrane-bound state is clearly different from the soluble state at the N terminus but is more similar for the middle and C-terminal portions of helix 1. Fig. 4*C* is a plot of the bimane probe mobility and represents a comparison between the membrane-associated (○) and soluble state (●) of $p190H_6$. Probe mobility was calculated as the inverse of the observed fluorescence anisotropy. Overall the patterns of the two profiles are similar. However, the probe mobility for the membrane-associated mutant proteins is generally lower than that for the soluble state. The mobility of bimane tethered to the N-terminal sites of helix 1 is rather low and shows a discontinuity with respect to the corresponding $\lambda_{em,\,max}$ values (Fig. 2, *A* and *B*). The reduction in the probe mobility of this region within helix 1 in the membrane-associated state may be caused by the strong binding of the proximal hexahistidine tag adjacent to the N terminus of helix 1.

Quantum Yield—Table 2 summarizes the bimane fluorescence quantum yield values for all helix 1 mutant proteins in both the soluble and membrane-associated states. The quantum yield of bimane-labeled mutants in the soluble state ranged between 0.05 and 0.24 and showed site-specific variations. In contrast, as expected, the bimane quantum yields for the membrane-associated mutant proteins were generally greater in magnitude and ranged between 0.12 and 0.52. In the soluble state, bimane tethered at sites D350C, A351C, V353C, F355C, Y356C, Q357C, and Q359C showed unusually low Q_F values. As shown in Table 2, the Q_F values of these mutants ranged between 0.05 and 0.12. These Q_F values are significantly lower than the value observed for Cys-bimane (0.18) in aqueous solution and thus cannot be explained simply on the degree of solvent exposure. Therefore, the reduced Q_F values of these mutant proteins suggest the presence of intrinsic fluorescence quenching mechanism(s) within the vicinity of the tethered fluorophores at these helix 1 sites. In earlier studies, Kosower *et al.* (33) and Farrens and co-workers (43) showed that a proximal aromatic residue, Trp, and to a lesser extent Tyr strongly quenched bimane fluorescence (32, 33). The colicin E1 $p190H_6$ channel domain consists of three Trp residues (Trp-424, Trp-460, and Trp-495; Fig. 1*A*). However, these Trp residues are not sufficiently close to the Cys-scanned sites within helix 1 in the soluble state of the protein. However, it can be seen from the 2.5-Å resolution x-ray structure of the $p190H_6$ that several Tyr residues are located within quenching distance of these sites within helix 1 (data not shown). Among the candidate quenchers are Tyr-434, Tyr-356, Tyr-363, and Tyr-367 (Fig. 1*B*). Tyr-434 is located within helix 5_b with its side chain projecting toward the N terminus of helix 1, and it forms part of the tertiary contact between helix 1 and helix 5_b. In addition, the phenolic side chain of Tyr-434 is also proximal to Phe-355 and Tyr-356. As part of the central core residues of helix 1, Tyr-356 is also in close proximity to Phe-355 and Gln-357. Similarly, the side chains of Tyr-363 and Tyr-367 project toward the interior of the protein where they are in close proximity to Gln-359. Therefore, the suppressed bimane Q_F values of D350C, A351C, V353C, F355C, Y356C, Q357C, and Q359C could be attributed to fluorescence quenching originating from a number of Tyr residues within helix 1 and 5_b.

Although most of the bimane quenching caused by intrinsic tertiary interaction with Tyr residues will likely be alleviated by unfolding of the protein upon binding to the membrane, the overall profile of the observed Q_F values for the membrane-associated mutants will still suffer from quenching effects imposed by Tyr-356 and Tyr-363. In order to eliminate these internal quenching effects and obtain meaningful Q_F profiles that can be used for secondary structure analysis (see below), we also report in Fig. 5, *A* and *B*, respectively, the relative Q_F values and ΔQ_F obtained for the membrane-bound bimane-labeled proteins. Although the inherent problem of internal quenching effects is still reflected in both of these plots, closer inspection of both of these Q_F profiles exhibit patterns that are in agreement with the periodicity of the steady-state fluorescence $\lambda_{em,\,max}$ and the fluorescence anisotropy (Fig. 2*C*, Fig. 4, and Fig. 5, *A* and *B*).

Dual Quenching Analysis of $p190H_6$ Helix 1—To characterize further the topology of the helix, the relative bilayer depth or surface exposure of each fluorophore was compared using the recently reported dual quenching method (26, 27, 34). In these experiments, the extent of bimane quenching at each site by a quencher species that resides primarily in the aqueous solution is compared with the quenching by one located within the bilayer. KI and 10-DN were used as water-soluble and membrane-embedded quenchers, respectively. As shown earlier, the quenching ratio (Q ratio) of a such a pairing system is very sensitive to the depth of the probed site, with a low Q ratio indicating a probe location near or at the center of the bilayer, whereas a high ratio reflects a location near the bilayer surface (26, 27, 34). Furthermore, this method allows the detection of heterogeneous orientation populations through the presence of quencher-induced $\lambda_{em,\,max}$ shifts (26, 27).

Fig. 6 shows the results of quenching analysis of the bimane-labeled helix 1 mutants of $p190H_6$ with KI as the water-soluble quencher and 10-DN as the membrane (hydrophobic) quencher. Fig. 6*A* is a histogram showing the extent of quenching by KI (*filled bars*) and also by 10-DN (*empty bars*). It is readily apparent that most of the bimane sites (Cys residues) within helix 1 are more accessible to KI than to the 10-DN quencher. Furthermore, the helical periodicity in the quenching analysis data were consistent with those observed for the fluorescence $\lambda_{em,\,max}$, anisotropy, and quantum yield measurements. The Q ratio

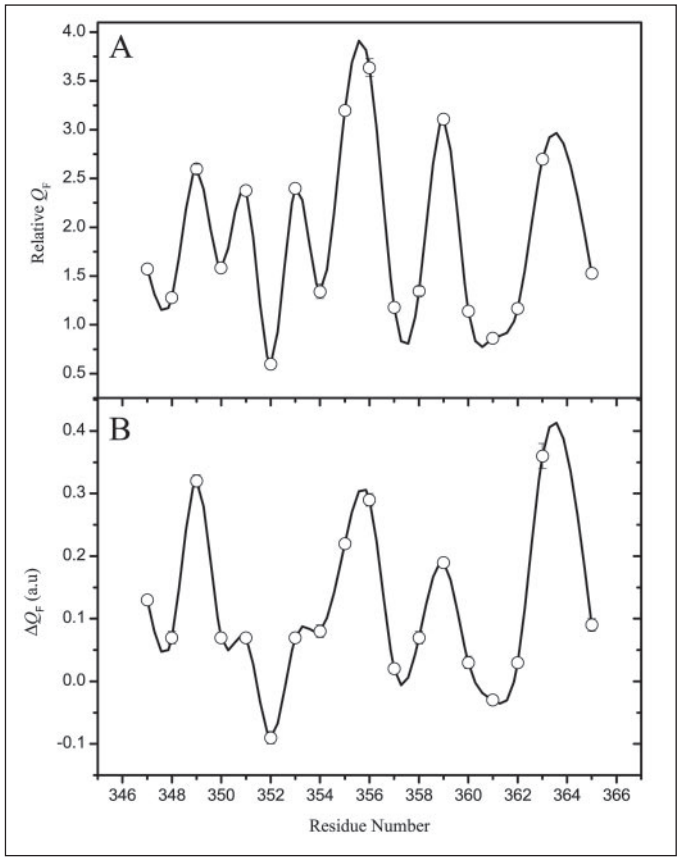

FIGURE 5. **Changes in fluorescence quantum yield (Q_F) of the bimane-labeled Cys mutants of colicin E1 channel domain upon binding to LUVs.** *A,* the relative Q_F of the bimane-labeled Cys mutants upon binding to LUVs. Relative Q_F is calculated as the ratio of the membrane-associated state (Q_{F-m}) and the solution state (Q_{F-s}) quantum yield values (Table 3) of the bimane-labeled Cys substituted sites (relative $Q_F = Q_{F\text{-}m}/ Q_{F\text{-}s}$). *B,* the difference in the ΔQ_F of the bimane-labeled Cys mutants in the membrane-associated and soluble states ($\Delta Q_F = Q_{F-m} - Q_{F-s}$).

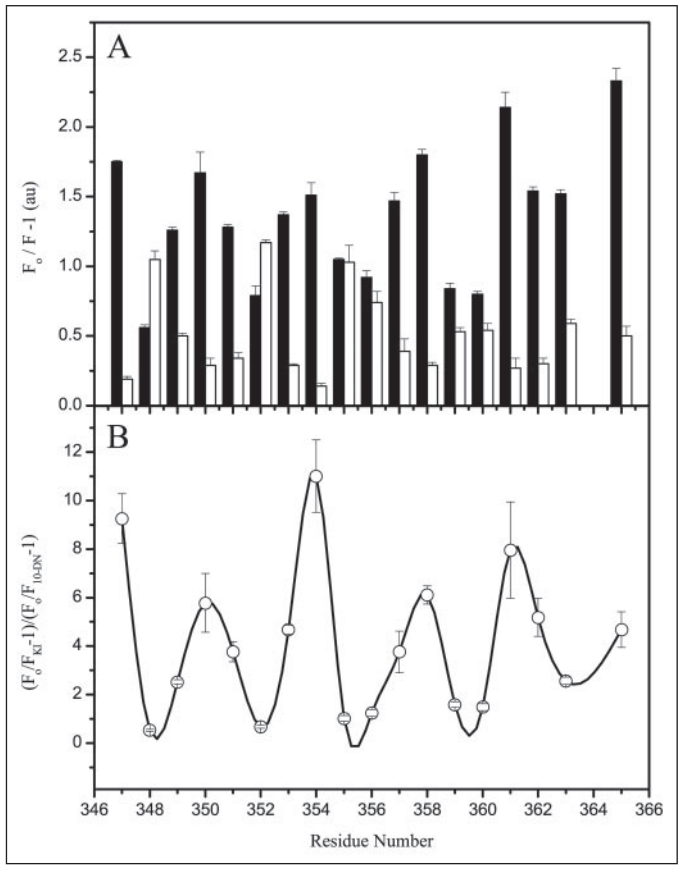

FIGURE 6. **Relative membrane bilayer depth for bimane-labeled p190H$_6$ helix 1 mutant peptides incorporated into lipid vesicles.** *A,* histogram showing the extent of bimane fluorescence quenching by KI (*black bar*) and by 10-DN (*empty bar*). *B,* a plot of the quenching ratio ($(F_o/F_{KI}) - 1)/((F_oF_{10\text{-}DN}) - 1$) (*Q* ratios) for bimane tethered at various Cys sites within helix 1. The samples contained 7.5 μg of bimane-labeled p190H$_6$ peptide in vesicles composed of 100 μM lipid in 130 mM NaCl, 20 mM dimethylglutaric acid buffer, pH 4.0. Average values and standard deviations for triplicates are shown.

gives a relatively simple and unambiguous determination of the depth of protein-tethered fluorophores in model membranes (26, 27). The data shown in Fig. 6*B* indicate that residues A348C, V349C, T352C, Y355C, Y356C, L359C, T360C, and Y363C have low *Q* ratio values and thus are relatively buried within the membrane bilayer. In contrast, residues A347C, D350C, A351C, V353C, S354C, Q357C, T358C, E361C, K362C, and E365C are moderately or largely exposed to the aqueous medium, according to the dual quencher analysis. Measurements of bimane $\lambda_{em,\,max}$ shifts in the presence and absence of both quenchers showed no significant quencher-induced λ_{em} shifts for all residues (data not shown), indicating a rather homogeneous orientation of the helix with respect to the bilayer.

Predicting Secondary Structure from Fluorescence Parameters—It is well known that protein segments that form amphipathic α-helices have periodic variation in the polar/nonpolar distribution along the segment with 3.6 residues per turn. The nature of the scale used to assign the hydrophobicity values to the amino acid residues will affect the display of periodicity, but the general pattern usually remains. We used the method of Cornette *et al.* (29) to analyze the various observed fluorescence parameters as well as the SASA for helix 1 of the colicin channel domain (Table 3). It is clear from this analysis, which detects the periodicity based on a least squares harmonic wave function analysis of the data, that helix 1 in the soluble channel domain is amphipathic. It yields a calculated residue per turn periodicity (*p*) (for SASA, $\lambda_{em,\,max}$, apparent polarity, and *r*) between 3.6 and 3.9, average = 3.7 ± 0.1 (3.6–3.7 is the standard observation for an amphipathic α-helix). It also yields an angular frequency of the periodicity (ω) between 92.8 and 98.8°, average = 96.5 ± 3.3° (the amphipathic helix is usually centered on 97.5°). Remarkably, when the analysis was applied to the helix 1 data for the membrane-associated channel domain, it was also evident that helix 1 maintains its amphipathic character when membrane-bound (Table 3) with an average *p* value of 3.7 ± 0.1 residues per turn and ω value of 97 ± 3.0° as judged by SASA, $\lambda_{em,\,max}$, apparent polarity, *r*, $\tau_{av\text{-}1}$, *Q* ratio, ΔQ_F, and relative Q_F.

DISCUSSION

Binding of the colicin E1 channel peptide to anionic lipid membranes at low pH results in profound conformational changes of the water-soluble structure leading to the formation of a membrane-bound "closed channel" precursor. Kinetic studies of the structural events associated with the initial membrane binding process have revealed four distinguishable events (21). These events are characterized as follows: binding → unfolding → helix elongation → bilayer insertion (21). The unfolding pathway of the protein as it contacts with model membranes has been shown to involve the following ordered sequence of events: (i) exposure of the hydrophobic core helices (8 and 9), resulting from the rearrangement of these helices with respect to the peripheral amphipathic helices; (ii) separation of helix 1 from the rest of the molecule followed by the expansion away from the core helical hairpin by helices 3, 4, 6, and 7 and finally helix 5; and (iii) slow condensation of the

TABLE 3
Summary of nonlinear least squares harmonic wave function analysis of the observed fluorescence parameters

Parameters	Soluble			Membrane-associated		
	p^a (rpt)	ω^b (degrees)	Residues[c]	p (rpt)	ω (degrees)	Residues
SASA	3.8	94.7	350–362	3.7	96.1	347–362
$\lambda_{em, max}$	3.7	98.0	350–362	3.8	95.8	347–362
Apparent polarity	3.6	98.8	350–362	3.6	101.2	350–362
r	3.9	92.8	350–362	3.8	94.1	351–358
Q ratio				3.7	98.3	347–362
$D\Phi_F$				3.6	100.3	353–362
Relative Φ_F				3.7	96.1	347–362
Average	3.7 ± 0.1	96.5 ± 3.3		3.7 ± 0.1	97.0 ± 3.0	

[a] rpt indicates the residues per turn periodicity of the parameters.
[b] ω indicates the angular frequency of the periodicity.
[c] Residues indicate which parameters were used in the fitting process.

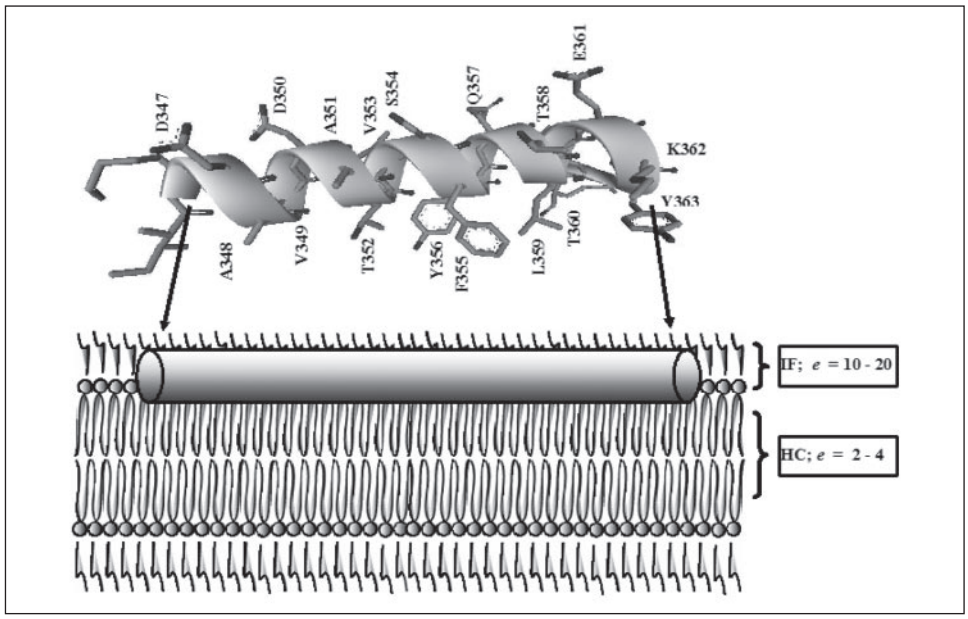

FIGURE 7. **Schematic representation of membrane-bound topology of helix 1.** Shown on the *top panel* is the ribbon diagram with side chains of the residues of helix 1 in the soluble protein. The overall helical boundary of this region of the protein remains unchanged upon binding to the membrane. This helix lies on the surface of the membrane with its nonpolar face bathing the hydrocarbon portion of the bilayer (*lower panel*). On the basis of our previous measured distance for the W355F mutant (13), the helix backbone is expected to localize within the interfacial layer of the membrane. The residues that make up the two phases of the amphipathic α-helix are also *highlighted*. Also shown are the accepted dielectric constants (ϵ) of the interfacial layer (*IF*; $\epsilon = 10–24$) and the hydrophobic core of the acyl chain (*HC*; $\epsilon = 2–4$).

surface-bound helices (35). Such massive structural reorganization of colicin E1 upon membrane contact would be expected to facilitate the membrane insertion of the core hydrophobic helices (helices 8 and 9) as the sequestering helical layers fold outward, much like the opening of an umbrella onto the surface of the membrane.

A large number of studies involving a wide array of experimental techniques and approaches have been used in the past to elucidate the topology of the membrane-bound colicin channel protein. Important components of the model(s) for the closed channel state include a monomeric species that features an extended two-dimensional helical hairpin array anchored by a single transmembrane helical hairpin (helices 8 and 9) that flickers between two states, a shallow and a deeper state (13, 14, 17–20, 36–38). Although most of these studies relied upon a global survey of the overall topology of the colicin E1 channel domain, a comprehensive "residue by residue" topological map of the protein in its membrane-bound state has been lacking. An exception is the SDSL-EPR study of Salwinski and Hubbell (39) where a series consisting of 23 consecutive single cysteine substitution mutants involving the 402–424 region of the colicin E1 channel peptide was investigated. In that study, the 402–424 region, which encompasses helices 4 and 5a (Fig. 1, *A* and *B*), was shown to form an extended and partially buried single α-helix of 19 residues including region 402–420 (39).

The site-directed fluorescence labeling data presented herein provide compelling evidence for the amphipathic nature of helix 1 when bound to the membrane bilayer (Fig. 7*A*). It is clear from the harmonic wave function analysis of the fluorescence data that the periodicity and angular frequency of helix 1 have not changed upon binding to the membrane surface. The data also support the large body of evidence that suggests that helix 1 lies on the surface of the membrane with its nonpolar face bathing the hydrocarbon portion of the bilayer. In previous global survey studies involving single Trp mutant channel peptides, we have shown that Trp substituted for Phe-355 was shallowly localized in the membrane and penetrated 10.6 Å from the bilayer center and only 4.4 ± 2 Å below the C-2 fatty acyl carbon (13, 17). Given the size (5 Å) of the indole ring of Trp residues, the measured distance is expected to localize the helix backbone of this region within the interfacial layer of the membrane. Such a conclusion is consistent with the observed increased protease accessibility of the Ala-336 to Lys-382 segment of the membrane-bound closed channel state of the protein (38). Our present data, which provide a residue by residue description of the position and bilayer depth of helix 1, reinforce these earlier studies and preclude the possibility that part of this helix is packed against or on top of another helix in the closed channel state.

The dual quencher analysis (Fig. 6) is a simple measure of the relative bilayer depth of a fluorophore, and this method was used to scan the bilayer penetration depth of helix 1. The results from this analysis were in excellent agreement with those from $\lambda_{em, max}$, apparent polarity, fluorescence anisotropy, and fluorescence quantum yield (Table 3), thus

providing strong evidence that helix 1 is appressed to the membrane surface and is parallel to the bilayer surface. Fig. 7 shows a simple model of helix 1 in the closed channel state.

The structure and the composition of the mature open channels formed by colicins upon voltage imposition have been enigmatic in nature. In general, it is widely accepted, on the basis of the bulk of available data, that the voltage-gated open channel contains a monomeric channel structure with an even-number of transmembrane helices consisting of both the N and C termini lying on the *cis* side of the membrane and movement of substantial segments of the membrane-bound precursor across the membrane. Two of the transmembrane helices are located within the hydrophobic helical hairpin (anchor) formed by helices 8 and 9 of the soluble protein. With respect to the identity of the remaining transmembrane peptide segments, various models have been presented, all of which indicated the formation of at least two additional transmembrane helices (15, 17, 38, 40, 41). Several of these models include an extended helix formed by the expansion of helices 1 and 2 of the soluble structure as one of the remaining transmembrane helices. Although helix extension is an integral component of the mechanism of colicin E1 membrane association and the rearrangements of the helices of the soluble protein have been documented in the membrane-bound state (39), our current data preclude the blending of helices 1 and 2 into an extended helix as a feature of the closed channel state of colicin E1 and possibly the structure of the open channel state. These results favor the toroidal model for the colicin E1 channel proposed earlier by Cramer and co-workers (22, 23), which requires shorter transmembrane helices (16 rather than 20 residues) and necessitates the involvement of phospholipids in an inverted micelle local membrane conformation in order to form a viable channel with a minimal amount of polypeptide (monomeric colicin). The toroidal lipid pore model has been used to explain the mechanism of cytotoxic activity of antimicrobial peptides (22), and this model suggests a direct role for membrane lipid in the formation of membrane pores by the peptides. An important requirement for the toroidal model is the sensitivity of the pore-forming activity to membrane lipid curvature, where lipids with positive spontaneous curvature stimulate while lipids having negative curvature inhibit pore formation of the antibiotic peptides. Recently, Cramer and co-workers (23) conclusively demonstrated the sensitivity of colicin E1 pore-forming activity on membrane curvature giving credence to a toroidal pore model for this bacteriocin.

The harmonic wave function analysis of our fluorescence data shows consistent discontinuity of the periodicity of all profiles beyond Lys-362, both in the soluble and membrane-bound states of the protein. In the x-ray crystal structure of colicin E1, Lys-362 marks the C terminus of helix 1 and the beginning of the short turn (Lys-362 to Glu-365) that separates helix 1 from helix 2 (Fig. 1, *A* and *B*). Furthermore, Gly-364 is conserved in all channel-forming colicins and is located in the short turn region that separates helix 1 and 2 in all known structures of channel-forming colicins. Accordingly, our data suggest that the helical boundaries of helix 1, at least at the C-terminal region, remain unaffected upon binding to the surface of the membrane. As such, our data refute earlier models that suggested the extension of parts of helix 1 and 2 into a single long amphipathic transmembrane helix as part of the mature open channel state. Such conclusions are supported by the recent findings from the comparison of the channels formed by the full-length colicin Ia and A (41). In this study, segments of both proteins that correspond to helix 1 of the soluble colicin Ia were shown to be inserted into the membrane with the loop between helix 1 and 2 forming a pivotal point between the transmembrane and translocated segments of the open channel state (41). For colicin A, this short loop is found to be partially exposed to the *trans* side of the membrane, and the majority of helix 2 is translocated across the membrane. Obviously, there still exists considerable controversy as to the nature and structure of both the close and open states of the pore-forming colicins. In order to continue our pursuit of the details of the colicin channel, we will continue our research to elucidate residue by residue the membrane structure of colicin E1 in its closed channel state and ultimately its open channel state. It is anticipated that this approach will help to clarify some of these ambiguities and the enigma that currently define the structure of this channel.

Our experience in using the mBBr reagent to label Cys residues within the colicin E1 channel domain indicates that the product Cys-bimane is a small and effective probe for evaluating protein structure and also for membrane protein topology (33, 42). This probe is relatively nonperturbing to protein structure and is sufficiently ambivalent to allow for its partitioning into the membrane bilayer at varying depths and consequently in a wide range of dielectric constants. We have also extended the earlier studies of Farrens and co-workers (32, 43) in the application of the observed fluorescence parameters of protein-tethered bimane to evaluate the topology of membrane-associated proteins. In our analysis, we observed that the bimane fluorescence lifetime and quantum yield parameters did not yield patterns that can easily be ascribed to a given secondary structure, but these parameters can reveal site-specific information concerning tertiary structure contacts. It is our hope that we can use these patterns in the future to define the constraints of the overall topology of the colicin E1 channel domain when in the membrane-bound state by various approaches, including fluorescence resonance energy transfer analysis.

Acknowledgment—We thank Dr. Zahir Husain for valuable assistance in the early stages of this research project.

REFERENCES

1. Pugsley, A. P. (1984) *Microbiol. Sci.* **1,** 203–205
2. Cramer, W. A., Dankert, J. R., and Uratani, Y. (1983) *Biochim. Biophys. Acta* **737,** 173–193
3. Stroud, R. M., Reiling, K., Wiener, M., and Freymann, D. (1998) *Curr. Opin. Struct. Biol.* **8,** 525–533
4. Lakey, J. H., and Slatin, S. L. (2001) *Curr. Top. Microbiol. Immunol.* **257,** 131–161
5. Gillor, O., Kirkup, B. C., and Riley, M. A. (2004) *Adv. Appl. Microbiol.* **54,** 129–146
6. Cramer, W. A., Heymann, J. B., Schendel, S. L., Deriy, B. N., Cohen, F. S., Elkins, P. A., and Stauffacher, C. V. (1995) *Annu. Rev. Biophys. Biomol. Struct.* **24,** 611–641
7. Riley, M. A., and Wertz, J. E. (2002) *Annu. Rev. Microbiol.* **56,** 117–137
8. Brunden, K. R., Cramer, W. A., and Cohen, F. S. (1984) *J. Biol. Chem.* **259,** 190–196
9. Taylor, R., Burgner, J. W., Clifton, J., and Cramer, W. A. (1998) *J. Biol. Chem.* **273,** 31113–31118
10. Dankert, J. R., Uratani, Y., Grabau, C., Cramer, W. A., and Hermodson, M. (1982) *J. Biol. Chem.* **257,** 3857–3863
11. Elkins, P., Bunker, A., Cramer, W. A., and Stauffacher, C. V. (1997) *Structure* (*Camb.*) **5,** 443–458
12. Cramer, W. A., Zhang, Y. L., Schendel, S., Merrill, A. R., Song, H. Y., Stauffacher, C. V., and Cohen, F. S. (1992) *FEMS Microbiol. Immunol.* **5,** 71–81
13. Palmer, L. R., and Merrill, A. R. (1994) *J. Biol. Chem.* **269,** 4187–4193
14. Shin, Y. K., Levinthal, C., Levinthal, F., and Hubbell, W. L. (1993) *Science* **259,** 960–963
15. Merrill, A. R., and Cramer, W. A. (1990) *Biochemistry* **29,** 8529–8534
16. Strawbridge, K. B., Palmer, L. R., Merrill, A. R., and Hallett, F. R. (1995) *Biophys. J.* **68,** 131–136
17. Tory, M. C., and Merrill, A. R. (1999) *J. Biol. Chem.* **274,** 24539–24549
18. Tory, M. C., and Merrill, A. R. (2002) *Biochim. Biophys. Acta* **1564,** 435–448
19. Zakharov, S. D., Lindeberg, M., Griko, Y., Salamon, Z., Tollin, G., Prendergast, F. G., and Cramer, W. A. (1998) *Proc. Natl. Acad. Sci. U. S. A.* **95,** 4282–4287
20. Kim, Y., Valentine, K., Opella, S. J., Schendel, S. L., and Cramer, W. A. (1998) *Protein Sci.* **7,** 342–348
21. Zakharov, S. D., Lindeberg, M., and Cramer, W. A. (1999) *Biochemistry* **38,**

11325–11332
22. Zakharov, S. D., Kotova, E. A., Antonenko, Y. N., and Cramer, W. A. (2004) *Biochim. Biophys. Acta* **1666,** 239–249
23. Sobko, A. A., Kotova, E. A., Antonenko, Y. N., Zakharov, S. D., and Cramer, W. A. (2004) *FEBS Lett.* **576,** 205–210
24. Musse, A. A., and Merrill, A. R. (2003) *J. Biol. Chem.* **278,** 24491–24499
25. Fletcher, A. N. (1969) *Photochem. Photobiol.* **9,** 439–444
26. Caputo, G. A., and London, E. (2003) *Biochemistry* **42,** 3265–3274
27. Hayashibara, M., and London, E. (2005) *Biochemistry* **44,** 2183–2196
28. Fraczkiewicz, R., and Braun, W. (1998) *J. Comput. Chem.* **19,** 319–333
29. Cornette, J. L., Cease, K. B., Margalit, H., Spouge, J. L., Berzofsky, J. A., and DeLisi, C. (1987) *J. Mol. Biol.* **195,** 659–685
30. Fridd, S. L., Gokce, I., and Lakey, J. H. (2002) *Biochimie* (*Paris*) **84,** 477–483
31. Heymann, J. B., Zakharov, S. D., Zhang, Y. L., and Cramer, W. A. (1996) *Biochemistry* **35,** 2717–2725
32. Mansoor, S. E., McHaourab, H. S., and Farrens, D. L. (1999) *Biochemistry* **38,** 16383–16393
33. Kosower, E. M., Giniger, R., Radkowsky, A., Hebel, D., and Shusterman, A. (1986) *J. Phys. Chem.* **90,** 5552–5557
34. Zhao, G., and London, E. (2005) *Biochemistry* **44,** 4488–4498
35. Lindeberg, M., Zakharov, S. D., and Cramer, W. A. (2000) *J. Mol. Biol.* **295,** 679–692
36. Lambotte, S., Jasperse, P., and Bechinger, B. (1998) *Biochemistry* **37,** 16–22
37. Malenbaum, S. E., Merrill, A. R., and London, E. (1998) *J. Nat. Toxins* **7,** 269–290
38. Zhang, Y. L., and Cramer, W. A. (1992) *Protein Sci.* **1,** 1666–1676
39. Salwinski, L., and Hubbell, W. L. (1999) *Protein Sci.* **8,** 562–572
40. Abrams, C. K., Jakes, K. S., Finkelstein, A., and Slatin, S. L. (1991) *J. Gen. Physiol.* **98,** 77–93
41. Slatin, S. L., Duche, D., Kienker, P. K., and Baty, D. (2004) *J. Membr. Biol.* **202,** 73–83
42. Sato, E., Sakashita, M., Kanaoka, Y., and Kosower, E. M. (1988) *Bioorg. Chem.* **16,** 298–306
43. Mansoor, S. E., McHaourab, H. S., and Farrens, D. L. (2002) *Biochemistry* **41,** 2475–2484